https://doi.org/10.5194/hess-2019-217
Preprint. Discussion started: 4 June 2019

Hydrology and Earth System Sciences
Discussions

Identification of Hotspots of Rainfall Variation Sensitive to Indian Ocean Dipole Mode through Intentional Statistical Simulations

Jong-Suk Kim[1], Phetlamphanh Xaiyaseng[1], Lihua Xiong[1], Sun-Kwon Yoon[2,*], Taesam Lee[3,*]

[1] State Key Laboratory of Water Resources and Hydropower Engineering Science, Wuhan University, Wuhan, 430072, P.R. China; jongsuk@whu.edu.cn (J.K.); lar99@yahoo.com (P.X.); xionglh@whu.edu.cn (L.X.)

[2] Department of Safety and Disaster Prevention Research, Seoul Institute of Technology, Seoul 03909, Republic of Korea

[3] Department of Civil Engineering, ERI, Gyeongsang National University, 501 Jinju-daero, Jinju, Gyeongnam, South Korea, 660-701

[*] Correspondence: skyoon@sit.re.kr (S.Y.); tae3lee@gnu.ac.kr (T.L.)

Abstract. This study analyzed the sensitivity of rainfall patterns over the Indochina Peninsula (ICP) to sea surface temperature in the Indian Ocean based on statistical simulations of observational data. Quantitative changes in rainfall patterns over the ICP were examined for both wet and dry seasons to identify hotspots sensitive to ocean warming in the Indo-Pacific sector. Rainfall variability across the ICP was confirmed amplified by combined and/or independent effects of the El Niño–Southern Oscillation and the Indian Ocean Dipole (IOD). During the years of El Niño and a positive phase of the IOD, rainfall is less than usual in Thailand, Cambodia, southern Laos, and Vietnam. Conversely, during the years of La Niña and a negative phase of the IOD, rainfall throughout the ICP is above normal, except in parts of central Laos and northern Vietnam. This study also simulated the change of ICP rainfall in the wet and dry seasons according to intentional IOD changes, and IOD-sensitive hotspots were

https://doi.org/10.5194/hess-2019-217
Preprint. Discussion started: 4 June 2019

Hydrology and Earth System Sciences Discussions
Open Access

verified through quantitative analysis. The results of this study provide clear understanding both of the sensitivity of regional precipitation to the IOD and of the potential future impact of statistical changes regarding the IOD in terms of understanding regional impacts associated with precipitation in a changing climate.

Keywords: Rainfall variability, Indian Ocean Dipole, ENSO, IBB simulation

1. Introduction

Spatiotemporal variation in precipitation extremes can result from amplification of changes in atmosphere–ocean interactions and intensification of the hydrological cycle on both regional and global scales attributable to the effects of global climate change (Allan and Soden, 2008; Kim and Jain, 2011; Ge et al., 2017; Kang et al., 2017; Kim et al., 2017; Gao et al., 2019). Changes in the magnitude and frequency of regional rainfall are related closely to the occurrence of floods and droughts. They have important implications not only in terms of their socioeconomic impact, but also in relation to the management of local and/or regional hydropower, irrigation, and environmental water resources (Chi et al., 2016; Gu et al., 2017; Choi et al., 2018). The occurrence of extreme precipitation, which is highly likely to continue into the future, is increasingly regarded as an area of concern by the public because many countries have experienced such extreme events in recent years (Croitoru et al., 2013; IPCC, 2013; Hirsch and Archfield, 2015; Chi et al., 2016; Donat et al., 2016). In particular, there has been rapid increase in both the amount of damage and the number of fatalities associated with the occurrence of extreme rainfall in developing countries because of their vulnerable infrastructure, high density of human activities, and poor practices of land use and development (Mirza, 2003; Yin et al., 2011).

https://doi.org/10.5194/hess-2019-217
Preprint. Discussion started: 4 June 2019

The El Niño–Southern Oscillation (ENSO) is known for its active and predictable short-term behavior within the global climate system (Chen and Cane, 2008), characterized by irregular but periodic change in the behavior of winds and sea level temperatures over the tropical eastern Pacific Ocean. Since the 2000s, new forms of El Niño have appeared more frequently in the central Pacific (Ashock and Yamagata, 2009; Pradhan et al., 2011). However, little is yet known about the causes of these new types of El Niño, some of which have been reported to have noticeable effect on the supply of warm seasonal freshwater and hydrological extremes in Pacific Rim countries (Kim et al., 2012; Yoon et al., 2013; Son et al., 2014; Wang et al., 2014; Kim et al., 2017). Research over the past two decades has identified a distinct climate anomaly in the Indian Ocean, known as the Indian Ocean Dipole (IOD) (Piechota et al., 1998; Saji et al., 1999; Mahala et al., 2015; Lqbal and Hassan, 2018). The IOD is an atmosphere–ocean coupling mode characterized by the opposition of anomalies of sea surface temperature (SST) in the west and east of the tropical Indian Ocean (Piechota et al., 1998; Saji et al., 1999; Webster et al., 1999). A positive (negative) IOD pattern is characterized by water warmer (cooler) than normal in the western tropical Indian Ocean (10° S–10° N, 50°–70° E) and water cooler (warmer) than normal in the southeastern tropical Indian Ocean (10° S to the equator, 90°–110° E). These events usually begin around May or June and they terminate rapidly in early winter after reaching a peak between August and October (Saji et al., 1999). Long-term climatic change has high correlation with large-scale atmospheric teleconnections and it has been reported predictable in relation to the behavior of nonlinear climate systems, particularly in terms of ocean-related climatic drivers such as ENSO and the IOD mode (Piechota et al., 1998; Saji et al., 1999). ENSO and IOD patterns are known as leading causes of large atmospheric change and they are related closely to seasonal variations in

https://doi.org/10.5194/hess-2019-217
Preprint. Discussion started: 4 June 2019

precipitation in the Indian Ocean region and around the world (Ashok et al., 2001; Ashok et al., 2003; McFadden et al., 2006; Pradhan et al., 2011).

Recent studies have suggested that the observed slowdown in the rise of global mean surface atmospheric temperature is related closely to the considerable transport of heat from the Pacific Ocean into the Indian Ocean via the Indonesian Throughflow (Kosaka and Xie, 2013; Lee et al., 2015; Liu et al., 2016; Zhang et al., 2018). Investigation of Indo-Pacific thermocouples can help both to improve understanding of regional-scale climatic variability that is globally relevant and to diagnose quantitatively such variability in a changing climate (Zhang et al., 2018). However, there has been little previous quantitative research on rainfall variation across the Indochina Peninsula (ICP) in relation to IOD phenomena and ENSO evolution. Therefore, based on historical observations, this study undertook quantitative analysis of the changes in SST in the Indo-Pacific sector and the associated interseasonal variation of precipitation over the ICP. The study had three primary areas of interest: (1) the spatiotemporal changes in magnitude and frequency of precipitation during the dry and wet seasons, (2) the relationship between the changes in weather extremes and large-scale climatic patterns over the ICP, and (3) identification of IOD-sensitive hotspots using the intentionally biased bootstrapping (IBB) technique based on limited historical observations.

2. Data and Methods

2.1. Precipitation Dataset and Climate Change Indices

This study used the high-resolution (0.5° × 0.5°) daily Climate Prediction Center Global Unified Precipitation dataset for 1979–2018, which was obtained from the website of NOAA's Earth System Research Laboratory's Physical Research Division

https://doi.org/10.5194/hess-2019-217
Preprint. Discussion started: 4 June 2019

(https://www.esrl.noaa.gov/psd/). The Global Precipitation Climatology Center monthly precipitation dataset with 1.0° × 1.0° spatial resolution for the period 1948–2018, which is based on quality-controlled data from 67,200 stations worldwide (Schneider et al., 2016), was also used to identify seasonal precipitation variability over the ICP region (5°–25° N, 90°–115° E) (Fig. 1). To identify changes in the frequency and intensity of rainfall, six major climate change indices (Karl et al., 1999) based on the daily Climate Prediction Center data from 1979–2018 were analyzed for both the wet season (May–October) and the dry season (November–April). These indices included the seasonal total precipitation (PRCPTOT) on wet days, seasonal total of the 95th percentile of precipitation (R95pTOT) on wet days (≥1.0 mm), seasonal maximum 1-day precipitation (RX1day), simple precipitation intensity index (SDII) with a daily precipitation amount on wet days of ≥1.0 mm, maximum number of consecutive dry days (CDD) with a daily precipitation amount of <1.0 mm, and maximum number of consecutive wet days (CWD) with a daily precipitation amount of ≥1.0 mm.

2.2. Indian Ocean Dipole (IOD) and El Niño–Southern Oscillation (ENSO)

The monthly SST anomaly (SSTA) from NOAA's Extended Reconstructed Sea Surface Temperature (ERSST) dataset v5 in the Tropical Indian Ocean (TIO) was used to calculate the IOD mode index. This is defined as the SSTA difference between the western (10° S–10° N, 50°–70° E) and southeastern (10° S to the equator, 90°–110° E) regions of the TIO (Saji et al., 1999). From 1948–2017, a 3-month running average was applied to the IOD mode index data (August–September–October), which is the peak phase period, with ±1σ to determine the years with positive and negative modes of the IOD (Fig. 2). To characterize different types of ENSO event, monthly

https://doi.org/10.5194/hess-2019-217
Preprint. Discussion started: 4 June 2019

Niño3 (5° S–5° N, 150° E–90° W) and Niño4 (5° S–5° N, 160° E–150° W) data for the period 1948–2018 were used for El Niño development phases (December–January–February). In this study, the pattern of El Niño was divided into two groups depending on where the peak and persistent anomalies in SST occurred in the tropical Pacific: (1) Eastern Pacific (EP); El Niño occurring in the EP and (2) Central Pacific (CP); El Niño emerging in the CP. This study employed two new indices (Eq. 1) to identify the two types of El Niño event through a simple transformation of the Niño3 and Niño4 indices, as proposed by Ren and Jin (2011):

$$N_{CT} = N_3 - \alpha N_4 \qquad \alpha = \begin{cases} 0.4, N_3 N_4 > 0 \\ 0, otherwise. \end{cases} \qquad (1)$$
$$N_{WP} = N_4 - \alpha N_3,$$

Here, N_3 and N_4 indicate the Niño3 and Niño4 indices, respectively.

Assessment of the relative impacts of the IOD and ENSO on rainfall across the ICP was based mainly on composite analyses. During 1979–2018, the effects of ENSO and the IOD were evaluated in terms of rainfall across the ICP during both the wet season (May–October) and the dry season (November–April).

2.3. Trend Detection

A nonparametric Mann–Kendall test is commonly used to detect a monotonic pattern in a time series of climate data based on the null hypothesis that the data are independent and sorted randomly (Mann, 1945; Kendall, 1990). The null hypothesis H_0 is random in the order of the sample data (X_i, $i = 1, 2..., n$) and it has no trend, whereas the alternative hypothesis H_1 represents the monotonous tendency of X. The S statistic for Kendall's tau is calculated as follows:

https://doi.org/10.5194/hess-2019-217
Preprint. Discussion started: 4 June 2019

$$S = \sum_{i=1}^{n-1}\sum_{j=i+1}^{n} \mathrm{sgn}(X_j\text{-}X_i) \tag{2}$$

and

$$\mathrm{sgn}(\_) = \begin{cases} 1 & \text{if}\ \_ > 0 \\ 0 & \text{if}\ \_ = 0\ . \\ -1 & \text{if}\ \_ < 0 \end{cases} \tag{3}$$

The S statistic is calculated using the following mean and variance:

$$E(S) = 0, \tag{4}$$

$$V(S) = \frac{n(n-1)(2n+5)\text{-}\sum_{m=1}^{n} t_m m(m-1)(2m+5)}{18}, \tag{5}$$

where t_m measures the ties of extent m. The standardized test statistic Z is estimated as follows:

$$Z = \begin{cases} \frac{S-1}{\sqrt{V(S)}} & S > 0 \\ 0 & S = 0. \\ \frac{S+1}{\sqrt{V(S)}} & S < 0 \end{cases} \tag{6}$$

The existence of autocorrelation in a dataset affects the probability of detecting a trend when it does not exist and vice versa, but this is often ignored. Thus, the modified nonparametric trend test developed by Hamed and Rao (1998) was applied in this study. The corrected Z value is derived as follows:

$$Z = \begin{cases} \frac{S-1}{\sqrt{V^*(S)}} & S > 0 \\ 0 & S = 0, \\ \frac{S+1}{\sqrt{V^*(S)}} & S < 0 \end{cases} \tag{7}$$

where

$$V^*(S) = V(S) * \frac{n}{n_S^*}, \tag{8}$$

https://doi.org/10.5194/hess-2019-217
Preprint. Discussion started: 4 June 2019

Hydrology and Earth System Sciences
Discussions

$$\frac{n}{n_S^*} = 1 + \frac{2}{n(n\text{-}1)(n-2)} * \sum_{i=1}^{n-1} (n\text{-}i)(n\text{-}i\text{-}1)(n\text{-}i-2)\rho_S(i) \quad , \quad (9)$$

where $\rho_S(i)$ is an autocorrelation function of the rank with respect to the observations. The sign of Z represents the trend direction and the magnitude of Z is associated with the significance level, where $|Z| > 1.64$ for the 10 % significance level and $|Z| > 1.96$ for the 5 % significance level.

2.4. Intentionally Biased Bootstrapping Method

Bootstrapping analysis is a statistical method that can generate replicated datasets from source data, and it can evaluate the variability of their quantiles without performing separate analytical calculations (Davision et al., 2003). However, the intentionally biased bootstrapping (IBB) technique applied in this study is a method that allows assessment of the relative effects of a response variable by deliberately increasing or decreasing the mean of the explanatory variable to a certain level while resampling it with the response variable (Lee, 2017). A brief description of the IBB analysis process is given below.

Among n observations x_i ($i = 1, 2, 3, \ldots, n$), suppose that the mean of the generated data is deliberately increased or decreased by $\Delta\mu$ for resampling of the observations with bootstrapping. As a result, high (low) values are likely to be resampled and low (high) values could be less likely to be selected. Thus, IBB can be obtained by allocating different weights $S_{i,n}$ depending on the following observation values (Eq. 10):

$$S_{i,n} = i \,/\, n. \quad (10)$$

https://doi.org/10.5194/hess-2019-217
Preprint. Discussion started: 4 June 2019

The weight $S_{i,n}$ assigned after scaling and adjustment contributes to the probability of selection for the data observed in the IBB procedure. The average of the resampled data can be expressed as in Eq. 11:

$$\tilde{\mu} = \frac{1}{\psi}\sum_{i=1}^{n} S_{i,n}\, x_i\ , \tag{11}$$

where x_i represents the i-th incremental value and $\psi = \sum_{i=1}^{n} S_{i,n}$. The average amount of increase or decrease $\Delta\mu$ is shown in Eq. 12:

$$\Delta\mu = \frac{1}{\psi}\sum_{i=1}^{n} S_{i,n}\, x_i - \frac{1}{n}\sum_{i=1}^{n} x_i. \tag{12}$$

To obtain another value of $\Delta\mu$, the weights can be regeneralized in order of weight sequence (r); thus, $\Delta\tilde{\mu}(r)$ is derived as follows:

$$\Delta\tilde{\mu}(r) = \tilde{\mu}(r) - \hat{\mu} = \frac{1}{\psi_r}\sum_{i=1}^{n} s_{i,n}^{r}\, x_i - \frac{1}{n}\sum_{i=1}^{n} x_i. \tag{13}$$

If the average value of increase or decrease is given as $\Delta\mu$, the weight "r" can be calculated accordingly. In this study, the selection of the weight sequence was performed using a Self-Organizing Migrating Algorithm (Zelinka, 2004) with the objective function to minimize $[\Delta\mu - \Delta\tilde{\mu}(r)]^2$. In addition, the IBB technique was employed to generate resampled datasets for the IOD and the response to the intensity and frequency of rainfall to identify IOD-sensitive hotspots over the ICP. The statistical significance of the analysis results was assessed using the significance level of the 95th percentiles.

3. Results

3.1. Seasonal Precipitation Patterns across the ICP

The ICP is a region in which monsoon rains occur in different seasons in association with seasonal winds and mountain areas. Geographically, the ICP has the Arakan

https://doi.org/10.5194/hess-2019-217
Preprint. Discussion started: 4 June 2019

Mountains in the west, the Bilauktung Mountains and the Dawna Mountains in the center, and the Annamese Mountains in the east. Meteorologically, the ICP is divided into three monsoon periods: the southwest monsoon during June–November, southeast monsoon during September–November, and northeast monsoon during November–February. This study considered the wet season (May–October) and the dry season (November–April) to identify the potential impact on regional rainfall associated with atmosphere–ocean feedback in the Indian and Pacific oceans.

Figure 3 shows the seasonal average precipitation during the wet and dry seasons across the ICP region during 1979–2018. The total precipitation during the wet season across the ICP is about 1000–1500 mm. In addition, it has been confirmed that precipitation variability is dependent on specific regions (Fig. 3a). The precipitation variability was found to differ significantly between inland (<1000 mm) and coastal areas (>2000 mm). Precipitation on the western coast of Cambodia, coast of western Thailand, and Myanmar during June–November is attributable to the influence of the southwest and southeast monsoons. Moreover, clear difference in precipitation is evident between eastern and western parts of the Arakan Mountains in Myanmar. As water vapor from Bangorman decreases over the mountains, the Arakan Mountains show an arid climate to the east and a pattern of strong precipitation to the west.

During the dry season, total precipitation across the ICP is about 150–200 mm, indicating that rainfall variability is not significantly dependent on specific regions (Fig. 3b). In particular, in the dry season, because of the influence of the northeast monsoon during November–February, high rainfall is received in central coastal areas of Vietnam, e.g., near the city of Danang. Similarly, in the case of Myanmar, eastern parts are dry because of the influence of the Arakan Mountains. The climatic characteristics of the ICP are distinctive not only because of the effects of monsoons

https://doi.org/10.5194/hess-2019-217
Preprint. Discussion started: 4 June 2019

and mountain areas, but also because of the characteristics of local areas and because of specific temporal effects. The precipitation patterns of the ICP are likely to change according to the characteristics of the wet and dry seasons, as well as because of the influence of ocean-related climate factors (e.g., the IOD and ENSO).

3.2. Spatiotemporal Variation in Precipitation over the ICP

Figures 4 and 5 illustrate the long-term trend of precipitation over the ICP during 1979–2018 for the wet and dry seasons, respectively. They show the results of the six major climate change indices that represent the magnitude and frequency of precipitation. For each figure, the direction of the trend is displayed in blue (increase) and red (decrease). Figures 4a, 4b, 5a, and 5b show the long-term trends of PRCPTOT and R95pTOT. These seasonal indices can be used to assess total precipitation. It can be seen that the characteristics of their spatial distribution are similar. During the wet season, there is a noticeable decrease in precipitation at the 5–10 % significance level in northern Cambodia, some parts of Laos, and southern Thailand. In addition, it can be seen that there is a marked trend of increase at the 5–10 % significance level in northwestern Myanmar, parts of western Thailand, central Vietnam, and southern parts of China (Fig. 4a and 4b).

During the dry season, there is a noticeable increase in precipitation at the 5–10 % significance level along eastern and southern coastal areas of the ICP (i.e., Vietnam and Cambodia) and some southern coastal regions of Thailand (Fig. 5a and 5b). The R95pTOT climate index also shows a trend of increase in precipitation to the west of the Arakan Mountains in Myanmar (Fig. 5b). Therefore, long-term changes in the pattern of precipitation across the ICP during the wet season show a trend of decrease (increase) in central inland areas (some coastal areas). During the dry season, there is a general trend of increase in precipitation across the ICP. Notably, the trend of increase in precipitation in southeastern coastal areas appears significant.

Figures 4c, 4d, 5c, and 5d illustrate the long-term trends in RX1day and SDII. The RX1day and SDII climate indices can be used to assess rainfall intensity. It can be seen that the characteristics of the spatial distribution of the two indices are similar. Moreover, the characteristics of their spatial distribution are also similar to PRCPTOT and R95pTOT. It can be seen that during the rainy season the intensity of rainfall in central and northern Myanmar, central and southern Vietnam, and southern China increases, whereas the rainfall intensity decreases in Laos, Cambodia, northeastern Myanmar, and South Vietnam. During the dry season, rainfall intensity generally increases across the ICP, although it shows a clear pattern of decrease in Laos, as in the wet season.

Figures 4e, 4f, 5e, and 5f show the long-term trends in CDD and CWD. The CDD and CWD indices can be used in assessment of droughts and floods, respectively. Therefore, it is unsurprising that the CDD and CWD indices exhibit opposite spatial distribution characteristics. During the rainy season, the CDD value across the ICP largely tends to increase, although it decreases in some coastal areas, e.g., Vietnam. The CWD index shows the reverse tendency.

During the dry season, an increase (decrease) of the CDD (CWD) index can be clearly observed at the 5–10 % significance level (Fig. 5e and 5f). The CDD index increases along the southeast coast of the ICP, e.g., in areas of Vietnam, Cambodia, and southern Thailand, whereas the CWD index exhibits the opposite trend. An increase (decrease) in the CDD index suggests that drought is more (less) likely to occur, while a decrease (increase) in the CWD index means that the occurrence of drought is less (more) likely. Therefore, during the rainy season, floods are expected to increase along

https://doi.org/10.5194/hess-2019-217
Preprint. Discussion started: 4 June 2019

Hydrology and Earth System Sciences
Discussions

the southeastern coast of the ICP (e.g., in Vietnam, Cambodia, and Thailand), while drought is more likely to occur during the dry season.

3.3. Precipitation Variability Associated with the IOD and ENSO

The IOD, Asian monsoon, and other regional climatological patterns can lead to local or global climate change, particularly in Indian Ocean Rim countries, which can cause severe flooding or droughts depending on IOD variability (Lqbal and Hassan, 2018). Composite analysis can clarify the role of the Southeast Asian Summer Monsoon in precipitation variability across the ICP region associated with years of strong IOD and ENSO, after identifying that tropical climate phenomena are the main factors that influence precipitation variability over the ICP during the wet and dry seasons. However, this role differs depending on the combination of the two climate phenomena and on the season.

Figure 6 shows the results of composite rainfall anomalies (shown as a percentage relative to normal) over the ICP during the wet and dry seasons in relation to the IOD and ENSO. The patterns of rainfall anomalies indicate significant difference between positive and negative IOD years. For positive IOD years, the wet season rainfall (Fig. 6a) shows a decrease of <20 % in southern parts of the ICP, whereas there is a marked increase in rainfall centered over the Arakan Mountains in western Myanmar. It can be seen that the amount of rainfall received during the dry season (Fig. 6c) is similar to that in the wet season, but there is 40–50 % less rainfall than usual in certain mainland regions of Southeast Asia, especially Yangon and Mawlamyine in Myanmar and in eastern Cambodia.

In negative IOD years, intense positive anomalies of rainfall can be seen in central Cambodia and southern parts of Vietnam. A slight strong-pitched anomaly pattern is evident during the wet season (Fig. 6b) around the coastline of both Bangladesh and Myanmar, whereas weak-pitched positive anomalies (about 10–15 % relative to the long-term average) are found throughout the ICP. However, changes in rainfall pattern are not evident during the dry season (Fig. 6d), and although the amount varies depending on region, rainfall is generally >30–50 % above the long-term average. As in the wet season, the dry season also shows relatively strong positive rainfall patterns with positive anomalies of >80–100 % in Cambodia and both central and southern Vietnam.

Sometimes droughts and flooding are likely to converge because of remote connections during IOD–ENSO periods, and they can have significant impact on the modulation of the large-scale oceanic and atmospheric environment, especially in the Indian Ocean and in Pacific Rim countries (Meza, 2013; Mahala et al., 2015; Lqbal and Hassan, 2018). Thus, consideration of both combined and independent effects of ENSO and the IOD on seasonal precipitation variability can provide improved predictive expertise, and reveal new insight into tropical climate change and global warming impacts (Ashok et al., 2001).

Figure 7 shows composite rainfall anomalies (November–April) during positive and negative IOD years that coincided with ENSO. During positive IOD and El Niño years (Fig. 7a), there is less rainfall than usual across Thailand, Cambodia, southern Laos, and Vietnam. In particular, southern regions of Myanmar (from Yangon to Mawlamyine) that border the Andaman Sea show a distinct decrease in rainfall by more than 50 % in comparison with the long-term mean (1981–2010). However, in contrast, there is 20–40 % more rainfall than usual in northern parts of the ICP, e.g., northern Myanmar, northeastern parts of Laos, and Vietnam. Furthermore, in Guangzhou in China, rainfall is up to 60 % higher in comparison with average years.

https://doi.org/10.5194/hess-2019-217
Preprint. Discussion started: 4 June 2019

These rainfall signals are stronger in WP El Niño years than in CT El Niño years (figures not shown). During negative IOD and La Niña years (Fig. 7b), rainfall above the long-term average is observed throughout the ICP, except for parts of central Laos and northern Vietnam. The pattern of increased rainfall appears strongly throughout Myanmar and regions around Ho Chi Minh City in Vietnam. However, in the region adjacent to India and Bangladesh, as well as the Shenzhen area of China, strong negative anomalies are evident.

3.4. Identification of IOD-Sensitive Hotspots through IBB Simulations

Section 3.3 discussed the significant impact on rainfall anomalies in the ICP attributable to the combined or independent effects of ENSO and the IOD. In particular, both positive IOD events and El Niño and negative IOD events and La Niña interact in modulating rainfall anomalies over the ICP. The IOD and ENSO are strongly correlated and their variations are mutually forced or triggered (Yu and Lau, 2005; Yuan and Li, 2008; Lestari and Koh, 2016). For the period 1979–2017, the correlation between the peak phase of the IOD and the two types of El Niño index proposed by Ren and Jin (2011) was analyzed. The results showed the IOD has strong positive correlation with the CT El Niño (N_{CT}) (ρ = 0.4850, p-value = 0.0018). However, the IOD also has positive correlation with the WP El Niño (N_{WP}), but not at a statistically significant level (ρ = 0.110, p-value = 0.5013). These results are also reflected in the results of the IBB simulation (Fig. 8). Figure 8 shows the results of 1000 simulations for the N_{CT} and N_{WP} indices performed by applying the IBB technique to the IOD index based on historical observations for the period 1979–2017. For applying a +1SD increase of the IOD, the mean difference between the observation of N_{CT} and simulated N_{CT} shows a statistically significant increase at the 95 % significance level (diff. = 0.392, Interquartile range (IQR) = 0.228). However, the difference in the mean value of the N_{WP} index, although increased slightly, is not statistically significant (diff. = 0.097, IQR = 0.094). For applying a −1SD decrease of the IOD, the simulation results show changes similar to the case with a +1SD increase of the IOD (N_{CT}: diff. = 0.360, IQR = 0.108, N_{WP}: diff. = 0.088, IQR = 0.098). Therefore, for changes in the IOD, the linear increase (or decrease) in the N_{CT} index is more pronounced than the change in the N_{WP} index.

The spatiotemporal connection between SST and winds shows strong coupling through precipitation and ocean dynamics (Saji et al., 1999). This dipole mode, accounts for about 12 % of SST variability in the Indian Ocean, and its duration of activity can greatly affect both the intensity and the frequency of rainfall in the Indian Ocean Rim countries, including the ICP. Based on statistical simulations of historical observations (1979–2018), Figs. 9 and 10 show rainfall variation and the most sensitive hotspot areas in the wet and dry seasons of the ICP attributable to IOD changes.

The spatial distribution of differences in PRCPTOT is shown in Fig. 9, given the condition of a ±1SD increase or decrease of the IOD in the wet season. For a +1SD increase of the IOD, PRCPTOT is >90 % higher than usual throughout Myanmar, and weak positive anomaly patterns are evident in southwestern China. In contrast, a pattern of decrease of PRCPTOT of 15–20 % less than the long-term average is evident in Cambodia and southern Vietnam, i.e., in areas of the downstream reaches of the Mekong River. However, no statistically significant changes occur in the central ICP region, except in some parts of central Laos and Thailand. This spatial distribution of rainfall anomaly is also found for the RX1day index, although occasional patterns of increase or decrease are evident and the spatial extent is reduced. In addition,

https://doi.org/10.5194/hess-2019-217
Preprint. Discussion started: 4 June 2019

throughout Myanmar, the CDD index is decreased by >25 % in comparison with the long-term average year, while the CWD index is increased by 35–50 %. For the CDD index, a statistically significant pattern of decrease is found across Vietnam, Cambodia, and Laos. The most significant changes in the CWD index are across Myanmar (increase of 35–50 %), southern Cambodia, and the southeast coast of Vietnam (decrease of 15–20 %). The other ICP regions generally show a pattern of weak increase in terms of CWD. For a −1SD decrease of the IOD, PRCPTOT, RX1day, and CWD all show distinct patterns of increase in the Laos and Vietnam basins, while the CDD index shows a predominant pattern of decrease, except in certain areas. Analysis indicates that other regions have a reverse pattern compared with the case of the +1SD increase of the IOD. Consequently, it is determined that changes in rainfall during the wet season in the ICP region are sensitive to changes in the IOD.

Given the condition of a ±1SD increase or decrease of the IOD for the dry season, the spatial distribution of the rainfall indices is shown in Fig. 10. For a decrease of −1SD of the IOD, there is more rainfall (PRCPTOT and RX1day) than usual throughout the ICP, especially in Laos and Vietnam. For a +1SD increase of the IOD, negative anomaly patterns of PRCPTOT are dominant in southern Vietnam, eastern Cambodia, and northeastern Thailand, while weak patterns of positive anomaly are evident in areas of Myanmar and South China. Compared with the changes in the rainfall indices during the wet season, changes in the rainfall indices are intensified and the spatial influence is more extensive. However, for the CDD and CWD indices, either the positive anomaly patterns are weakened or negative anomaly patterns appear for a +1SD increase of the IOD. Especially for the CWD index, a pattern of decrease by more than 10–20 % compared with the long-term average is found in Thailand, whereas the Myanmar region shows a pattern of increase of 15–25 %. In

https://doi.org/10.5194/hess-2019-217
Preprint. Discussion started: 4 June 2019

Hydrology and Earth System Sciences
Open Access
Discussions

this study, we simulated the changes in both wet and dry season rainfall across the ICP according to intentional IOD changes, and IOD-sensitive hotspots were verified through quantitative analysis. The findings of this study could help elucidate the long-term changes in rainfall expected in the ICP region in a changing climate.

4. Summary and Conclusions

This study analyzed changes in the magnitude and frequency of precipitation during the dry and wet seasons over the ICP, taking into account both the dipole mode in the tropical Indian Ocean and SST warming in the Pacific Ocean. The main results are summarized in the following.

1. According to analyses of the long-term trend in seasonal rainfall across the ICP during 1979–2018, rainfall showed significant decreases in northern Cambodia, parts of Laos, and southern Thailand during the wet season (May–October). Moreover, significant increases were evident in northwestern Myanmar, some parts of western Thailand, central Vietnam, and southern China. During the dry season (November–April), PRCPTOT rose noticeably in eastern and southern coastal areas of the ICP (i.e., Vietnam and Cambodia) and some southern coastal regions of Thailand.
2. During the wet season, the CDD index increased and decreased in some coastal areas such as Vietnam. However, during the dry season, increases in CDD and decreases in CWD were evident in the ICP. In particular, a pattern of decline in CWD dominated southeastern coastal areas of the ICP, including Vietnam, Cambodia, and southern Thailand.
3. The IOD showed strong positive correlation with the CT El Niño. However, although the IOD exhibited positive correlation with the WP El Niño, the

https://doi.org/10.5194/hess-2019-217
Preprint. Discussion started: 4 June 2019

relationship was not statistically significant. The variability of rainfall across the ICP was confirmed amplified by combined and independent effects of ENSO and the IOD. During years of positive IOD and El Niño, there was less rainfall than usual throughout Thailand and Cambodia, southern Laos, and Vietnam. In particular, the southern part of Myanmar, which borders the Andaman Sea, showed a decrease in regional rainfall of >50 % in comparison with the long-term average. In contrast, northern parts of India and China, including Myanmar, northeastern Laos, and Vietnam, received 20–40 % more rainfall than usual. Years with a negative IOD mode and La Niña showed rainfall above the long-term average across the ICP, except for certain parts, e.g., Central Laos and northern Vietnam.

4. Through application of the IBB technique, this study simulated the change of rainfall across the ICP for the wet and dry seasons according to intentional IOD changes, and IOD-sensitive hotspots were verified through quantitative analysis. For the wet season, a +1SD increase of the IOD resulted in >90 % more PRCPTOT than usual across Myanmar in the northwestern ICP. Conversely, in Cambodia and southern Vietnam, rainfall patterns were 15–20 % less than the long-term average in the region of the lower Mekong River. In addition, the CDD index decreased throughout Myanmar by >25 % compared with the long-term average. The most significant change in the CWD index was in Myanmar, i.e., a 35–50 % increase. However, a pattern of decrease appeared across the southeastern coast of the ICP in southern Cambodia and Vietnam. For a +1SD increase of the IOD in the dry season, negative anomaly patterns of PRCPTOT were found dominant in South Vietnam, eastern Cambodia, and northeastern Thailand, and more rainfall than usual occurred throughout the

ICP, especially in Laos and Vietnam, when considering a −1SD decrease of the IOD.

Although the results of this study are based on limited observations, they provide a clear perspective on the sensitivity of local precipitation to atmosphere–ocean interactions, and they reveal the potential future impact of statistical changes to the IOD, improving our understanding of the associated regional impact on precipitation under the effects of climate change.

Author contribution: conceptualization, J.K., S.Y., and T.L.; Formal analysis, J.K.; Methodology, T.L. and J.K.; resources, J.K. and L.X.; writing—original draft preparation, P.X., S.Y., and J.K.; writing—review and editing, L.X. and T.L.

Acknowledgments: This research is supported by the National Key R&D Program of China (2017YFC0405901), the National Natural Science Foundation of China (No. 51525902), and the Ministry of Education "111 Project" Fund of China (B18037), all of which are greatly appreciated.

Competing interests: The authors declare that they have no conflict of interest.

References

Allan, R.P. and Soden, B.J.: Atmospheric warming and the amplification of precipitation extremes, Science, 321(5895), 1481-1484, https://doi.org/10.1126/science.1160787, 2008.

https://doi.org/10.5194/hess-2019-217
Preprint. Discussion started: 4 June 2019

Ashok, K., Guan, Z., and Yamagata, T.: Impact of the Indian Ocean Dipole on the relationship between the Indian monsoon rainfall and ENSO, Geophys. Res. Lett., 28, 4499–4502, https://doi.org/10.1029/2001GL013294, 2001.

Ashok, K., Guan, Z., and Yamagata, T.: Influence of the Indian Ocean dipole on the Australian winter rainfall, Geophys. Res. Lett. 30, 1821, https://doi.org/doi:10.1029/2003GL017926, 2003.

Ashok, K. and Yamagata, T.: The El Niño with a difference, Nature, 461, 481-484, https://doi.org/10.1038/461481a, 2009.

Chi, X., Yin, Z., Wang, X., and Sun, Y.: Spatiotemporal variations of precipitation extremes of China during the past 50 years (1960–2009), Theor. Appl. Climatol., 124, 555–564, https://doi.org/10.1007/s00704-015-1436-8, 2016.

Croitoru, A.E., Chiotoroiu, B.C., Ivanova, Todorova V., AND Torică, V.: Changes in precipitation extremes on the Black Sea Western Coast, Glob. Planet Chang., 102, 10–19, https://doi.org/10.1016/j.gloplacha.2013.01.004, 2013.

Chen, D. and Cane, M.A.: El Niño prediction and predictability, J. Comput. Phys., 227, 3625–3640, https://doi.org/10.1016/j.jcp.2007.05.014, 2008.

Choi, J.H., Yoon, T.H., Kim, J.S., and Moon, Y.I.: Dam rehabilitation assessment using the Delphi-AHP method for adapting to climate change, Journal of Water Resources Planning and Management, 144(2), 06017007, https://doi.org/10.1061/(ASCE)WR.1943-5452.0000877, 2018.

Davison, A. C., Hinkley, D. V., and Young, G.A.: Recent developments in bootstrap methodology, Statistical Science, 18(2), 141-157, https://doi.org/10.1214/ss/1063994969, 2003.

Donat, M.G., Lowry, A.L., Alexander, L.V., O'Gorman, P.A., and Maher, N.: More extreme precipitation in the world's dry and wet regions, Nat. Climate Change, 6, 508–514, https://doi.org/10.1038/nclimate2941, 2016.

Gao, Q., Kim, J.S., Chen, J., Chen, H., and Lee, J.H.: Atmospheric Teleconnection-Based Extreme Drought Prediction in the Core Drought Region in China, Water, 11(2), 232, https://doi.org/10.3390/w11020232, 2019.

Ge, F., Zhi, X., Babar, Z.A., Tang, W., and Chen, P.: Interannual variability of summer monsoon precipitation over the Indochina Peninsula in association with ENSO, Theor. Appl. Climatol., 128(3–4), 523–531, https://doi.org/10.1007/s00704-015-1729-y, 2017.

Gu, X., Zhang, Q., Singh, V. P., and Shi, P.: Changes in magnitude and frequency of heavy precipitation across China and its potential links to summer temperature, J. Hydrol., 547, 718–731, https://doi.org/10.1016/j.jhydrol.2017.02.041, 2017.

Hamed, K.H. and Rao, A.R.: A modified Mann-Kendall trend test for autocorrelated data, J. Hydrol., 204(1–4), 182–196, https://doi.org/10.1016/S0022-1694(97)00125-X, 1998.

Hirsch, R.M. and Archfield, S.A.: Flood trends: Not higher but more often, Nat. Clim. Change, 5(3), 198, https://doi.org/10.1038/nclimate2551, 2015.

https://doi.org/10.5194/hess-2019-217
Preprint. Discussion started: 4 June 2019

IPCC, Climate change 2013: the physical science basis. Contribution of Working Group I to the Fifth Assessment Report of the Intergovernmental Panel on Climate Change. Cambridge University Press, UK, 2013.

Iqbal, A. and Hassan, S.A.: ENSO and IOD analysis on the occurrence of floods in Pakistan, Nat. Hazards, 91(3), 879–890, https://doi.org/10.1007/s11069-017-3158-y, 2018.

Karl, T. R., Nicholls, N. and Ghazi, A.: Clivar/GCOS/WMO workshop on indices and indicators for climate extremes workshop summary, in Weather and Climate Extremes, Asheville, North Carolina, pp. 3–7, 3-6 June, 1997.

Kang, H.Y., Kim, J.S., Kim, S.Y., and Moon, Y.I.: Changes in High-and Low-Flow Regimes: a Diagnostic Analysis of Tropical Cyclones in the Western North Pacific, Water Resources Management, 31(12), 3939-3951, https://doi.org/10.1007/s11269-017-1717-3, 2017.

Kendall, M.G., and Gibbons, J.D.: Rank correlation methods. Ed. Edward Arnold., London, England, 1990.

Kim, J. S. and Jain, S.: Precipitation trends over the Korean peninsula: typhoon-induced changes and a typology for characterizing climate-related risk, Environmental Research Letters, 6(3), 034033, https://doi.org/10.1088/1748-9326/6/3/034033, 2011.

Kim, J.S., Zhou, W., Wang, X., and Jain, S.: El Nino Modoki and the summer precipitation variability over South Korea: a diagnostic study, Journal of the

Meteorological Society of Japan. 90(5), 673-684, https://doi.org/10.2151/jmsj.2012-507, 2012.

Kim, J.S., Son, C.Y., Moon, Y.I., and Lee, J.H.: Seasonal rainfall variability in Korea within the context of different evolution patterns of the central Pacific El Niño, Journal of Water and Climate Change, 8(3), 412-422, https://doi.org/10.2166/wcc.2016.020, 2017.

Kosaka, Y. and Xie, S. P.: Recent global-warming hiatus tied to equatorial Pacific surface cooling, Nature, 501(7467), 403, https://doi.org/10.1038/nature12534, 2013.

Lee, S.K., Park, W., Baringer, M.O., Gordon, A.L., Huber, B., and Liu, Y.: Pacific origin of the abrupt increase in Indian Ocean heat content during the warming hiatus, Nature Geoscience, 8(6), 445, https://doi.org/10.1038/ngeo2438, 2015.

Lee, T.: Climate change inspector with intentionally biased bootstrapping (CCIIBB ver. 1.0)–methodology development, Geoscientific Model Development, 10(2), 525-536, https://doi.org/10.5194/gmd-10-525-2017, 2017.

Lestari, R.K. and Koh, T.Y.: Statistical evidence for asymmetry in ENSO–IOD interactions, Atmos. Ocean, 54, 498–504, https://doi.org/10.1080/07055900.2016.1211084, 2016.

Liu, W., Xie, S.P., and Lu, J.: Tracking ocean heat uptake during the surface warming hiatus, Nature Communications, 7, 10926, https://doi.org/10.1038/ncomms10926, 2016.

Mahala, B.K., Nayak, B.K., and Mohanty, P.K.: Impacts of ENSO and IOD on tropical cyclone activity in the Bay of Bengal, Nat. Hazards, 75, 1105–1125, https://doi.org/10.1007/s11069-014-1360-8, 2015.

Mann, H.B.: Nonparametric Tests Against Trend, Econometrica 13, 245–259, https://doi.org/10.2307/1907187, 1945.

McPhaden, M.J., Zebiak, S.E., and Glantz, M.H.: ENSO as an integrating concept in Earth Science, Science, 314, 1740–1745, https://doi.org/10.1126/science.1132588, 2006.

Meza, F.J.: Recent trends and ENSO influence on droughts in Northern Chile: an application of the standardized precipitation evapotranspiration index, Weather Clim. Extrem., 1, 51–58, https://doi.org/10.1016/j.wace.2013.07.002, 2013.

Mirza, M.M.Q.: Climate change and extreme weather events: can developing countries adapt? Clim. Pol., 3(3), 233–248, https://doi.org/10.3763/cpol.2003.0330, 2003.

Piechota, T.C., Chiew, H.S., Francis, Dracup J.A., and McMachon, T.A.: Seasonal streamflow forecasting in eastern Australia and the El Niño-Southern Oscillation, Water Res. Res. 34, 3035–3044, https://doi.org/10.1029/98WR02406, 1998.

Pradhan, P.K., Preethi, B., Ashok, K., Krishna, R., and Sahai, A.K.: Modoki, Indian Ocean Dipole, and western North Pacific typhoons: Possible implications for extreme events, J. Geophys. Res. 116: D18108, https://doi.org/10.1029/2011JD015666, 2011.

Ren, H.L. and Jin, F.F.: Nino indices for two types of ENSO, Geophys. Res. Lett., 38, L04704, https://doi.org/10.1029/2010GL046031, 2011.

Saji, N.H., B.N. Goswami, P.N. Vinayachandran and T. Yamagata.: A Dipole Mode in the tropical Indian Ocean, Nature, 401(23), 360363, https://doi.org/10.1038/43854, 1999.

Schneider, U., Ziese, M., Meyer-Christoffer, A., Finger, P., Rustemeier, E., and Becker, A.: The new portfolio of global precipitation data products of the Global Precipitation Climatology Centre suitable to assess and quantify the global water cycle and resources, Proc. IAHS, 374, 29-34, https://doi.org/10.5194/piahs-374-29-2016, 2016.

Son, C.Y., Kim, J.S., Moon, Y.I., and Lee, J.H.: Characteristics of tropical cyclone-induced precipitation over the Korean River basins according to three evolution patterns of the Central-Pacific El Niño, Stochastic Environmental Research and Risk Assessment, 28(5), 1147-1156, https://doi.org/10.1007/s00477-013-0804-0, 2014.

Wang, X., Zhou, W., Li, C.Y., and Wang, D.X.: Comparison of the impact of two types of El Niño on tropical cyclone genesis over the South China Sea, International Journal of Climatology, 34(8), 2651-2660, https://doi.org/10.1002/joc.3865, 2014.

Webster, P.J., Moore, A.M., Loschnigg, J.P., and Leben, R.R.: Coupled ocean–atmosphere dynamics in the Indian Ocean during 1997–98, Nature, 401, 356–360, https://doi.org/10.1038/43848, 1999.

Yin, J., Yin, Z.E., Zhong, H.D., Xu, S.Y., Hu, X.M., Wang, J., and Wu, J.P.: Monitoring urban expansion and land use/land cover changes of Shanghai

https://doi.org/10.5194/hess-2019-217
Preprint. Discussion started: 4 June 2019

metropolitan area during the transitional economy (1979–2009) in China, Environ Monit. Assess., 177(1–4), 609–621, https://doi.org/10.1007/s10661-010-1660-8, 2011.

Yoon, S.K., Kim, J.S., Lee, J.H., and Moon, Y.I.: Hydrometeorological variability in the Korean Han River Basin and its sub-watersheds during different El Niño phases, Stochastic Environmental Research and Risk Assessment, 27(6), 1465–1477, https://doi.org/10.1007/s00477-012-0683-9, 2013.

Yu, J.Y. and Lau, K.: Contrasting Indian Ocean SST variability with and without ENSO influence: a coupled atmosphere-ocean GCM study, Meteorol. Atmos. Phys., 90, 179–191, https://doi.org/10.1007/s00703-004-0094-7, 2005.

Yuan, Y. and Li, C.: Decadal variability of the IOD-ENSO relationship, Chin. Sci. Bull., 53, 1745–1752, https://doi.org/10.1007/s11434-008-0196-6, 2008.

https://doi.org/10.5194/hess-2019-217
Preprint. Discussion started: 4 June 2019

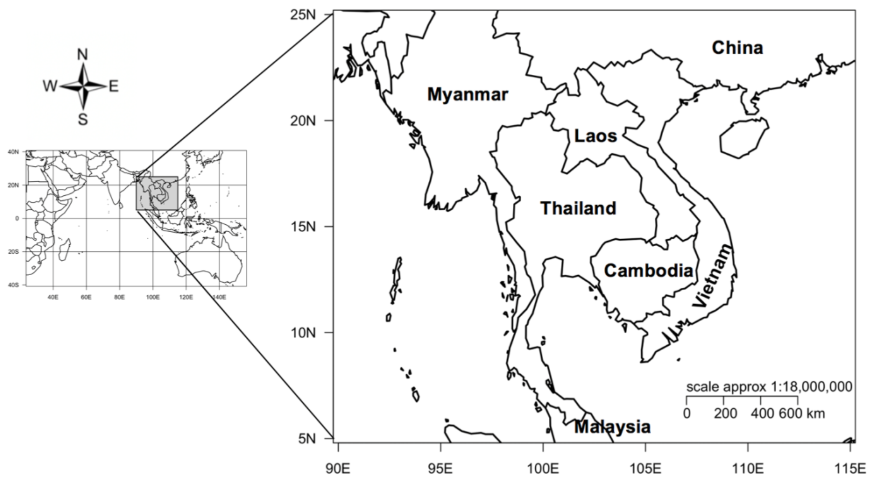

Figure 1. Map of the Indochina Peninsula (5°–25° N, 90°–115° E).

https://doi.org/10.5194/hess-2019-217
Preprint. Discussion started: 4 June 2019

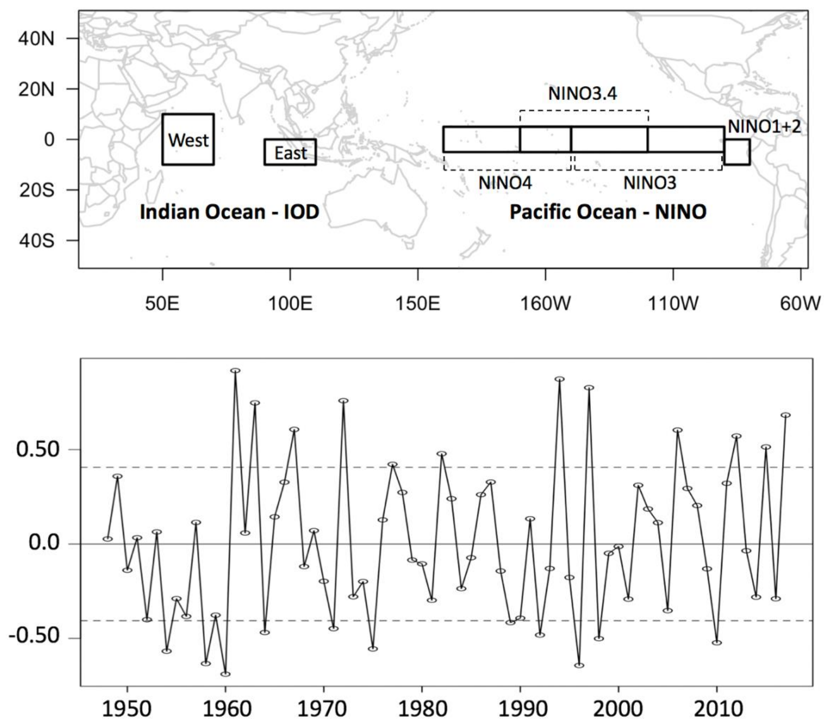

Figure 2. Dipole mode in the tropical Indian Ocean (TIO) and Niño region in the Pacific Ocean. The Indian Ocean Dipole (IOD) index is defined based on the sea surface temperature anomaly difference between the western (10° S–10° N, 50°–70° E) and southeastern (10° S to the equator, 90°–110° E) regions of the TIO shown in the upper panel. In the lower panel, the IOD time series during 1948–2017 is shown by the solid line, and the ±1SD of the IOD is marked by dotted lines.

https://doi.org/10.5194/hess-2019-217
Preprint. Discussion started: 4 June 2019

Hydrology and Earth System Sciences
Open Access
Discussions

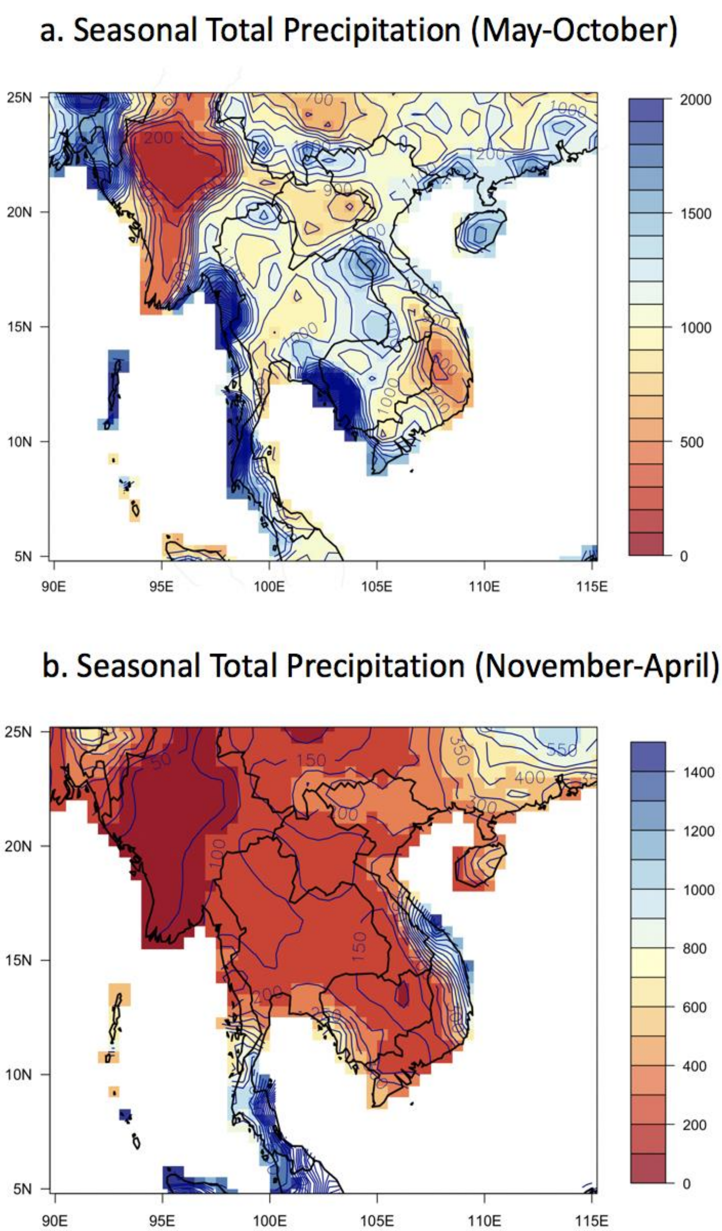

Figure 3. Average precipitation (mm) during the (a) wet and (b) dry seasons (1979–2018).

https://doi.org/10.5194/hess-2019-217
Preprint. Discussion started: 4 June 2019

Hydrology and Earth System Sciences
Discussions
Open Access

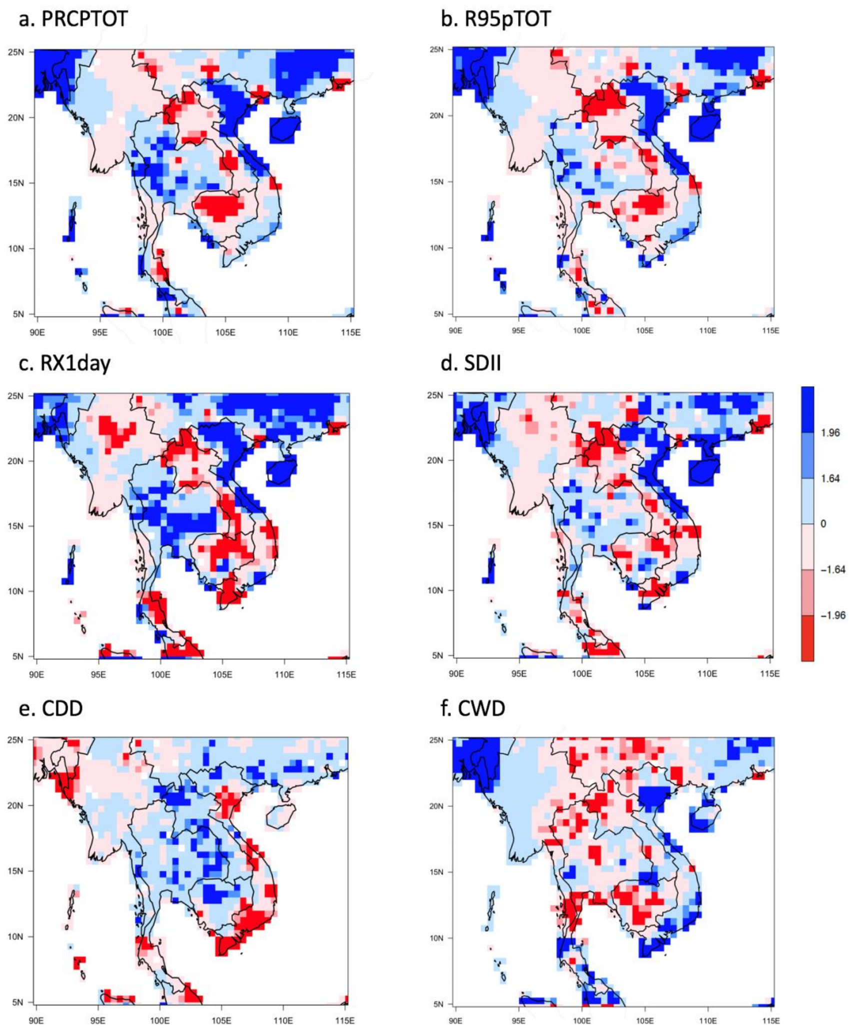

Figure 4. Long-term trend in seasonal precipitation for the wet season (May–October) over the ICP during 1979–2018. (a)–(f) show the analysis results of the six major climate change indices that reflect the magnitude and frequency of precipitation. In each panel, positive and negative trends are displayed in blue and red, respectively. The magnitude of Z is associated with the significance level, i.e., $|Z| > 1.64$ is for the 10 % significance level and $|Z| > 1.96$ is for the 5 % significance level.

Hydrology and Earth System Sciences
Open Access
Discussions

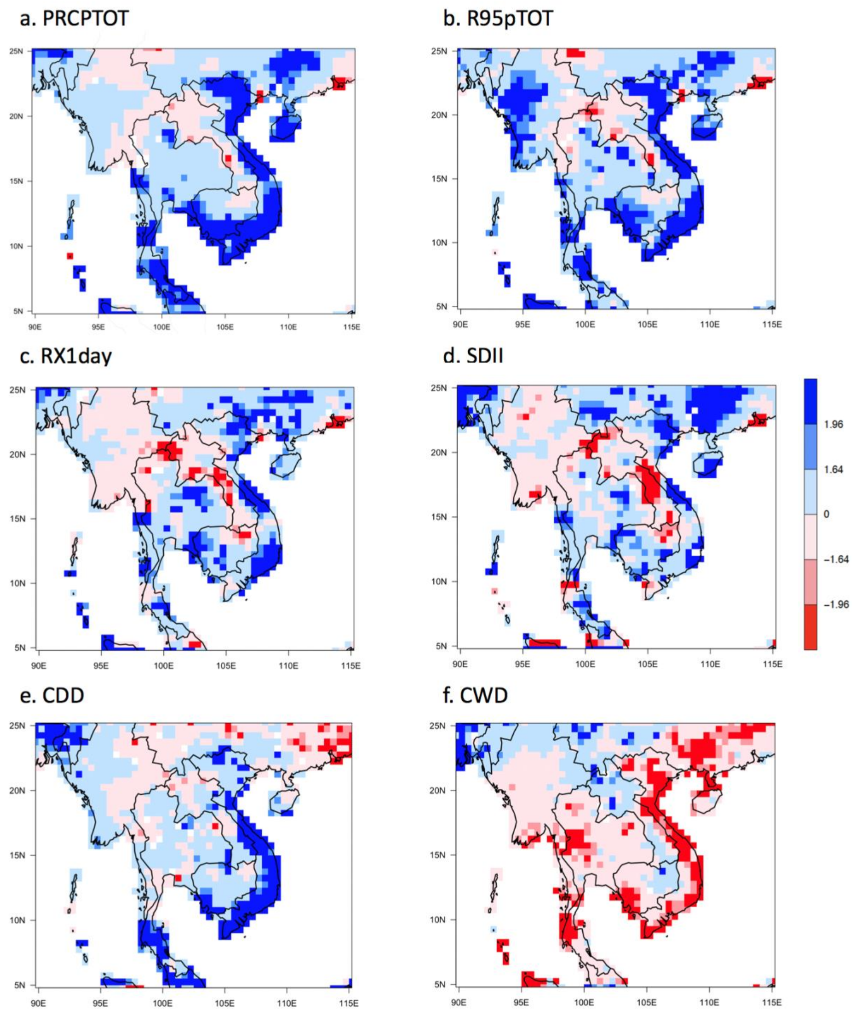

Figure 5. Same as Fig. 4 but for seasonal precipitation during the dry season (November–April).

https://doi.org/10.5194/hess-2019-217
Preprint. Discussion started: 4 June 2019

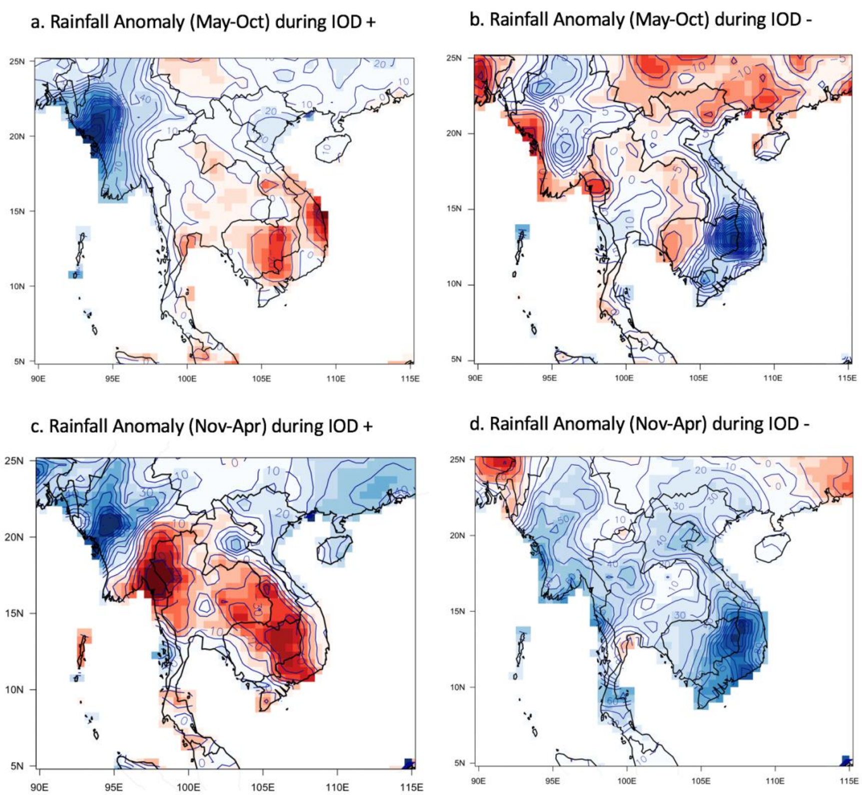

Figure 6. Composite of seasonal rainfall anomaly (%) during positive and negative IOD years: (a) rainfall anomaly in wet season during positive IOD years, (b) rainfall anomaly in wet season during negative IOD years, (c) rainfall anomaly in dry season during positive IOD years, and (d) rainfall anomaly in dry season during negative IOD years. Positive (negative) values show increasing (decreasing) rainfall departure from the long-term average (1981–2010).

https://doi.org/10.5194/hess-2019-217
Preprint. Discussion started: 4 June 2019

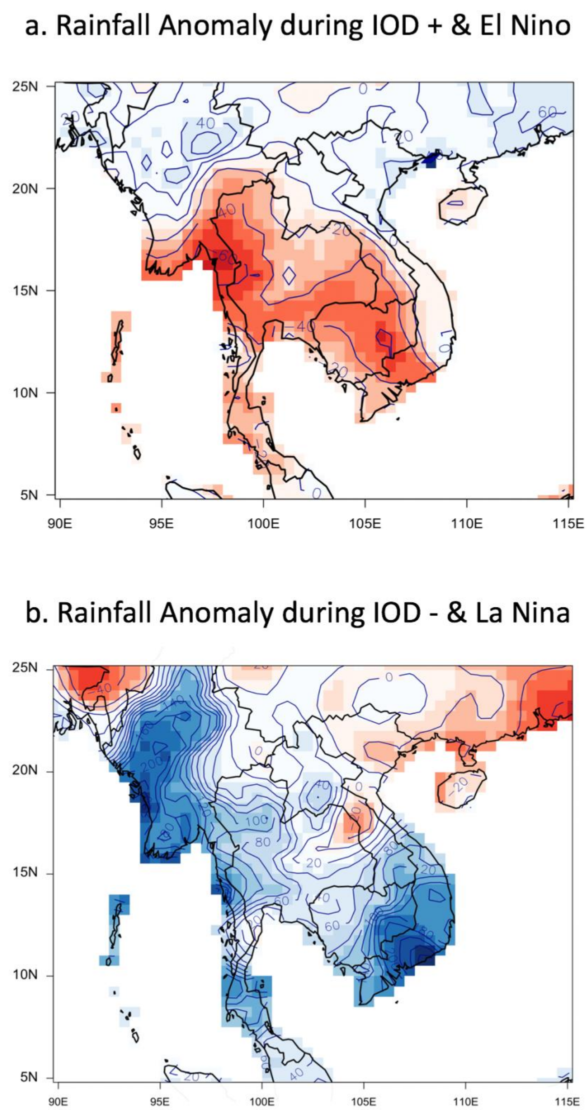

Figure 7. Composite rainfall anomaly in dry season (November–April) associated with the IOD and ENSO: (a) rainfall anomaly during years with positive IOD and El Niño, and (b) rainfall anomaly during years with negative IOD and La Niña. Positive (negative) values show increasing (decreasing) rainfall departure from the long-term average (1981–2010).

https://doi.org/10.5194/hess-2019-217
Preprint. Discussion started: 4 June 2019

Hydrology and Earth System Sciences
Open Access
EGU
Discussions

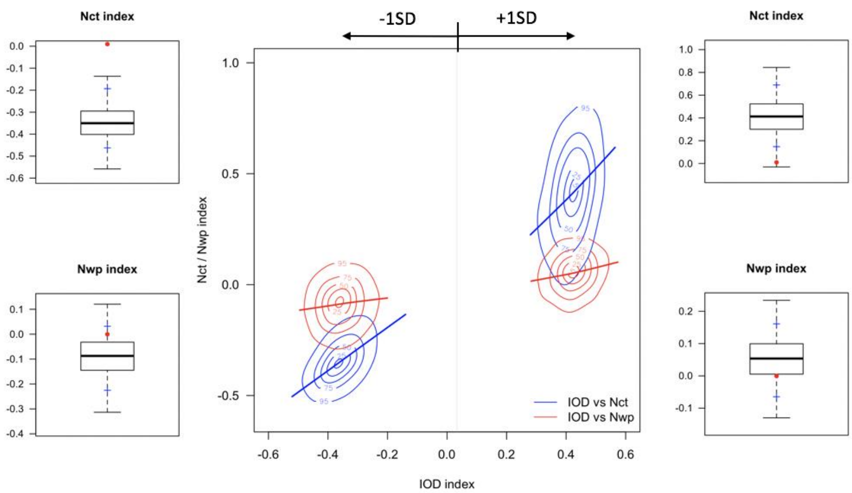

Figure 8. Mean differences of the two types of El Niño with ±1SD of the IOD. In the main panel, contours (5th, lower quadrant, median, upper volatile, and 95th level) summarize the IOD index and Nct or Nwp index using the intentionally biased bootstrapping model. Both left and right panels deliberately apply ±1SD of the IOD to show results of 1000 simulations for the Nct and Nwp indices. Red dots in each panel represent the average value of the observations.

https://doi.org/10.5194/hess-2019-217
Preprint. Discussion started: 4 June 2019

Hydrology and Earth System Sciences
Open Access
Discussions

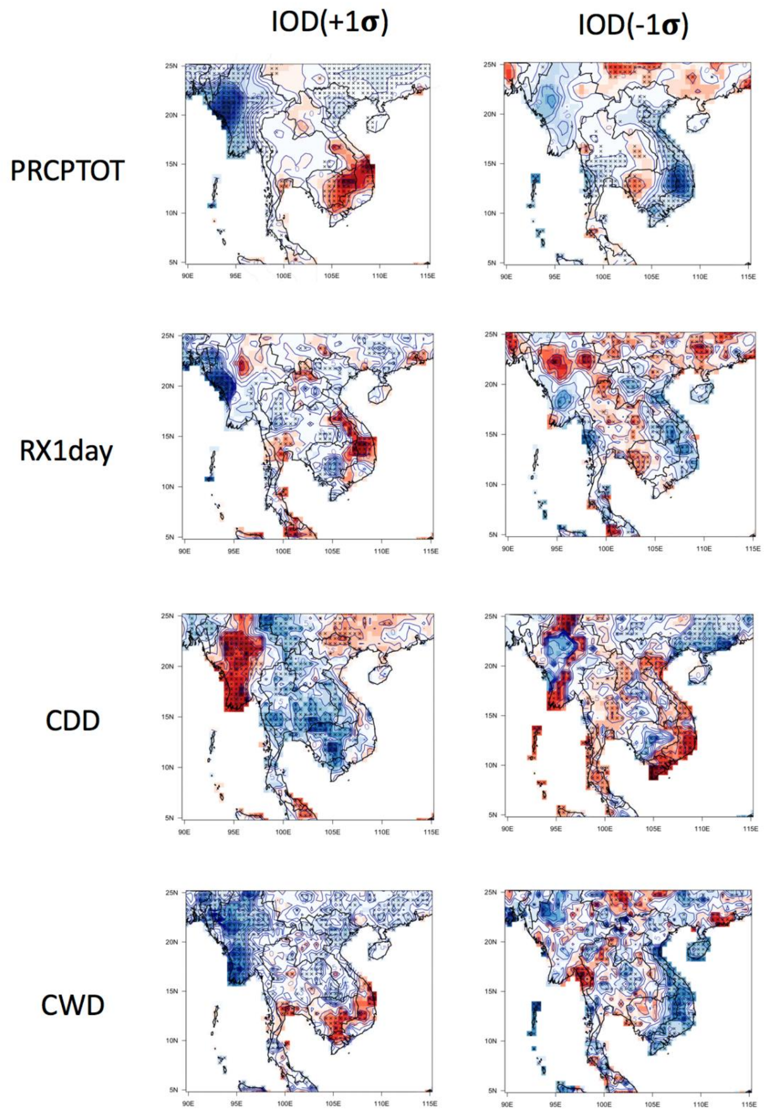

Figure 9. Spatial distributions of the percentage changes in major precipitation indices for the wet season (May–October) over the ICP region for intentional increases (+1SD) or decreases (−1SD) of the IOD index using the intentionally biased bootstrapping simulation. In each panel, the statistically significant area of change at the 95 % significance level is shown by an "x" symbol.

https://doi.org/10.5194/hess-2019-217
Preprint. Discussion started: 4 June 2019

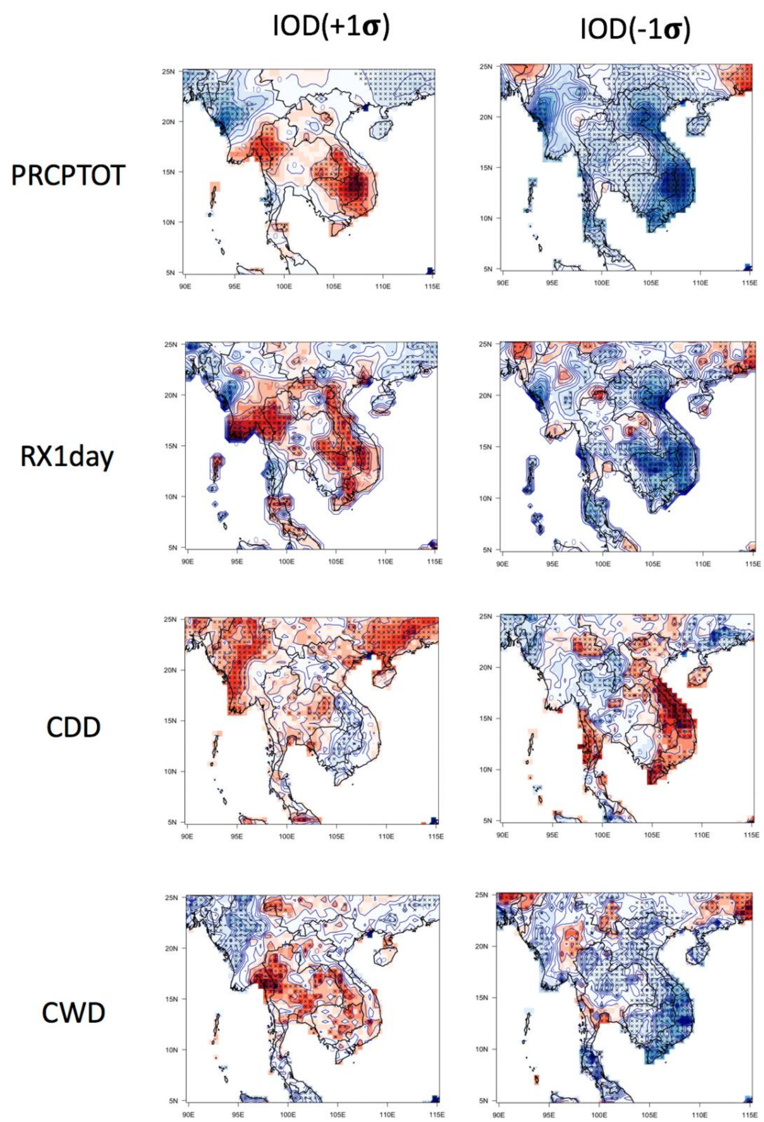

Figure 10. Same as Fig. 9 but for the dry season (November–April) over the ICP region.